Isothermal Crystallization Kinetics and Morphology Development of Isotactic Polypropylene Blends with Atactic Polypropylene

Jean-Hong Chen, Yu-Lun Chang

Department of Polymer Materials, Kun Shan University, Tainan 710, Taiwan, Republic of China

Received 20 March 2006; accepted 17 August 2006
DOI 10.1002/app.25354
Published online in Wiley InterScience (www.interscience.wiley.com).

ABSTRACT: The crystallization kinetics and morphology development of pure isotactic polypropylene (iPP) homopolymer and iPP blended with atactic polypropylene (aPP) at different aPP contents and the isothermal crystallization temperatures were studied with differential scanning calorimetry, wide-angle X-ray diffraction, and polarized optical microscopy. The spherulitic morphologies of pure iPP and larger amounts of aPP for iPP blends showed the negative spherulite, whereas that of smaller amounts of aPP for the iPP blends showed a combination of positive and negative spherulites. This indicated that the morphology transition of the spherulite may have been due to changes the crystal forms of iPP in the iPP blends during crystallization. Therefore, with smaller amounts of aPP, the spherulitic density and overall crystallinity of the iPP blends increased with increasing aPP and presented a lower degree of perfection of the γ form coexisting with the α form of iPP during crystallization. However, with larger amounts of aPP, the spherulitic density and overall crystallinity of the iPP blends decreased and reduced the γ-form crystals with increasing aPP. These results indicate that the aPP molecules hindered the nucleation rate and promoted the molecular motion and growth rate of iPP with smaller amounts of aPP and hindered both the nucleation rate and growth rate of iPP with larger amounts of aPP during isothermal crystallization. J Appl Polym Sci 103: 1093–1104, 2007

Key words: crystal structures; morphology; poly(propylene) (PP)

INTRODUCTION

It is well known that isotactic polypropylene (iPP) exhibits several crystalline forms, including α, β, and γ forms, at different process conditions. In all these, the crystal forms of iPP are identical and correspond to the familiar threefold helix at different stacking geometries of these helices.[1–15] This is because the crystal morphologies are affected not only by the molecular mass and molecular mass distribution of iPP but also by different blending compounds and preparation conditions, that is, isothermal temperature and pressure.[7,16–18]

The γ form of iPP was first reported during the 1960s and was generated by crystallization at elevated pressures of the polymer. However, Meille et al. reported[19] that the structure of the γ form did not account for the diffraction peak at $2\theta = 24.5^\circ$. They also reported a γ form generated at atmospheric pressure from low-molecular-weight iPP, which led to a reassignment of the structure as a modified triclinic unit cell. Contrary to this unit cell, the modified cell accounted for the diffraction peak at $2\theta = 24.5^\circ$ because the α angle of the lattice constants was higher in the modified triclinic cell.[20] The modified triclinic structure is unique and contains sheets of parallel molecules, but the molecular orientation between adjacent sheets becomes nonparallel every two sheets. The angle between the nonparallel and parallel sheets is about 81°; this angle is also observed at the contact planes between the radial lamellae and the branches of the α form.[21–23]

Recently, iPP blends have received much attention because the morphology, crystallinity (X_c), microstructure, and melting and crystallization behaviors of iPP are strongly dependent on the process conditions and blend components.[24–31] Time-resolved X-ray scattering techniques showing the relatively modest incorporation of atactic polypropylene (aPP) in the interlamellar regions, depending on the crystallization temperature (T_c) and blend composition were also reported by Wang et al.[25,26] However, they indicated that the partial miscibility of the aPP and iPP components in the blends resulting the crystallizability and crystal morphology of iPP was not a strong function of aPP and the segregation of aPP on size

Correspondence to: J.-H. Chen (kelvench@mail.ksu.edu.tw).

Contract grant sponsor: National Science Council of the Republic of China; contract grant number: NSC 93-2216-E-168-004.

TABLE I
Characteristics and Thermal Properties for the iPP Blended Samples

Materials	T_g (°C)[a]	T_c (°C)[b]	ΔH_c (J/g)[b]	T_m^L (°C)[c]	ΔH_f (J/g)[c]	T_m^o (°C)[a]	X_c (%)[d]
iPP-100	−10.1	129.0	83.7	163.5	109.6	187.2	53.7
iPP-90	−10.1	126.1	78.8	163.5	123.6	186.9	57.6
iPP-80	−10.3	127.6	72.6	163.7	132.0	186.4	61.3
iPP-70	−10.6	125.1	61.7	163.7	120.8	186.0	56.2
iPP-50	−10.4	123.1	62.7	162.7	102.7	184.6	41.2
iPP-30	−11.1	120.6	33.4	161.0	50.3	181.7	25.2

[a] T_g, Glass-transition temperature, and T_m^o, equilibrium melting temperature, were reported in reference 31.
[b] Calculated from the crystallization exotherm of the DSC cooling trace after melting.
[c] Calculated from the melting endotherm of the DSC melting trace of the isothermal crystallized iPP blend at 130°C.
[d] Calculated from the X-ray diffraction intensity pattern of the isothermal crystallized iPP blend at 130°C.

scales larger than the lamellar spacing. The segregation of aPP to a size scale larger than lamellar spacing was consistent with literature observations showing both open spherulitic morphologies and the pooling of aPP within the spherulitic morphology, depending on the crystallization conditions.[25,26] More recently, we[31] reported that aPP was locally miscible with iPP in the amorphous region of iPP/aPP blends and the contents of the γ form of iPP depended remarkably on both the aPP content and isothermal T_c. The effect of aPP addition on iPP was investigated by Keith and Padden;[32,33] they reported that with increasing aPP in iPP/aPP blends, a more open spherulitic texture was observed due to the incorporation of aPP diluent in the interfibrillar regions. Although the main structure of the iPP blends is similar to that of pure iPP, the morphology development of iPP blends has not yet been studied in detail. Therefore, study of the relationship between the aPP content and isothermal conditions and the morphology development of iPP blends is becoming more important. From this point of view, a study of the effect of process conditions on the crystallization kinetics of polymers is an important step in understanding, predicting, and designing microstructure formation under differences processes conditions of iPP blends. Generally, the crystallization kinetics of polymers have been well described by the Avrami equation, although they are limited when used to describe the crystallization of the polymers.[34,35]

In this study, the effect of aPP contents and isothermal temperature on the spherulitic morphology and isothermal crystallization kinetics of iPP blends were studied. The Avrami equation was used to analyze the isothermal crystallization kinetics of iPP blends. Dynamic differential scanning calorimetry (DSC) thermograms provided the thermal properties and necessary crystallization kinetics data in this study. Polarized optical microscopy (POM) and wide-angle X-ray diffraction (WAXD) results were also used to understand the morphology development of the iPP in blends under various conditions.

EXPERIMENTAL

Material preparation

iPP with a weight-average molecular weight of 1.9×10^5 g/mol and aPP with a weight-average molecular weight of 1.96×10^4 g/mol were purchased from Aldrich Chemical, USA. Melt-blended specimens of these homopolymers with various compositions were prepared with a twin-screw apparatus (MP2015, APV Chemical Machinery Co., USA) at 210°C. The iPP/aPP (w/w %) mixing ratios were 100/0, 90/10, 80/20, 70/30, 50/50, and 30/70; the blends were prepared and defined as iPP-100, iPP-90, iPP-80, iPP-70, iPP-50, and iPP-30, respectively. The composition and thermal properties of the iPP blends in this study are collected in Table I.

The compression-molded films were prepared by melt-pressing of iPP blends for a molding of $120 \times 120 \times 1$ mm^3. All samples were molten at 210°C and were held at this temperature for 10 min to allow compete melting, and then, these iPP blend molds were taken out and immediately submerged in a temperature-controlled compression-molding machine at different T_c's, with temperature intervals of 5°C from 90 to 135°C under a pressure of 50 kg/cm^2. They were then placed between the two steel platens and held at 120 min for necessary isothermal crystallization.

DSC measurement

Thermal behaviors of all of the isothermal crystallized iPP blends were measured with a differential scanning calorimeter (Perkin-Elmer Pyris Diamond DSC, USA; with an intracooler for the lowermost temperature of about −65°C). A sample weight of about 5 mg was cut from the isothermal crystallized iPP blends at different isothermal T_c's, put into a sample pan, and then melted in the furnace in a nitrogen atmosphere from 30 to 210°C at a rate of 10°C/min; then, the melting thermogram was measured. The temperature and area of the endothermic

TABLE II
Isothermal Crystallization Kinetics for the iPP Blended Samples

Sample	T_c (°C)	$t_{1/2}$ (min)	$\tau_{1/2}$ (min^{-1})	n	k (°C/min) × 10^3
iPP-100	110	0.25	4.00	3.50	18.3
	115	0.32	3.13	2.68	12.0
	120	0.41	2.44	2.76	7.82
	125	0.53	1.89	2.78	6.47
	130	0.76	1.32	2.65	5.86
	135	2.73	0.37	2.70	1.36
iPP-90	110	0.19	5.26	3.98	92.3
	115	0.22	4.55	3.24	79.8
	120	0.27	3.70	2.87	19.1
	125	0.34	2.94	2.67	23.8
	130	1.12	0.89	2.64	1.32
	135	5.89	0.17	3.48	0.56
iPP-80	110	0.14	7.14	4.12	24.7
	115	0.17	5.88	3.76	18.3
	120	0.34	2.94	3.43	10.3
	125	0.47	2.13	3.09	4.51
	130	1.08	0.93	2.46	15.3
	135	7.04	0.14	3.12	1.12
iPP-70	110	0.18	5.56	4.03	32.6
	115	0.21	4.76	4.09	23.4
	120	0.29	3.45	3.57	14.5
	125	0.82	1.22	3.22	6.73
	130	2.05	0.49	2.83	5.26
	135	7.05	0.14	2.32	1.64
iPP-50	110	0.20	5.00	4.17	40.7
	115	0.29	3.45	4.01	23.9
	120	0.55	1.82	2.56	9.56
	125	0.90	1.11	2.76	1.23
	130	2.45	0.41	2.34	3.18
	135	7.11	0.14	2.12	2.03
iPP-30	110	0.23	4.35	3.45	36.5
	115	0.33	3.03	2.97	11.1
	120	0.88	1.14	3.06	3.03
	125	2.71	0.37	3.10	0.83
	130	4.46	0.22	2.94	0.41
	135	9.25	0.11	2.86	0.27

peak were taken as the melting temperature and the heat of fusion (ΔH_f), respectively. The temperature was 210°C and was maintained for 10 min to eliminate any previous thermal history; then, the sample was cooled at a rate of 10°C/min, and the crystallization thermogram was measured. The temperature and area of the exothermic curve were taken as T_c and the latent heat of crystallization (ΔH_c), respectively. These measurement results are shown in Table I. The isothermal crystallization kinetics were also measured with the Pyris Diamond DSC. The samples were melted in the furnace in a nitrogen atmosphere at 210°C for 10 min to eliminate any previous thermal history, and then, they were rapidly cooled to T_c at a rate of 400°C/min and maintained at this temperature for the time necessary for isothermal crystallization. These isothermal crystallization kinetics data are listed in Table II.

POM measurement

The spherulite morphologies of the iPP blends were investigated with a polarized optical microscope (Zeiss Axioskop-40, UK, with a Linkam TH600 hot stage, Germany). The samples, inserted between two microscope cover glasses, were melted at 210°C and squeezed to obtain a sample about 10 μm thick for the iPP blend thin films. The thin-film samples were inserted into the hot stage. Each sample was melted at 210°C for 10 min to eliminate any previous thermal history; they were then cooled to isothermal T_c at a rate of 90°C/min and maintained at this temperature for the time necessary for crystallization.

WAXD measurement

WAXD intensity curves of isothermal crystallized iPP blends were measured with graphite-monochromatized Cu Kα radiation generated at 40 kV and 180 mA in a Rigaku D/Max 2500VL/pc diffractometer. WAXD intensities were recorded from $2\theta = 5$ to 35° with a continuous scanning speed of $2\theta = 1°$/min with data collection at each 0.02° of 2θ.

RESULTS AND DISCUSSION

Melting endotherm morphology

Figure 1(a–f) shows the DSC melting scans at a heating rate of 10°C/min for isothermal crystallized iPP blends at different isothermal T_c's. However, a general feature of these curves was the appearance of two melting endotherms at temperatures below 120°C; a single melting endotherm existed at temperatures above 120°C. As shown in Figure 1, with increasing aPP content, the heat of fusion of the lower temperature endotherm (ΔH_f^L) decreased, whereas the heat of fusion of the higher temperature endotherm (ΔH_f^H) increased. This result indicates that X_c and the morphology for the iPP blends after isothermal crystallization were affected by the aPP content and isothermal T_c. The decrease in ΔH_f^L with increasing aPP content was indicative of a decrease in recrystallization or reorganization of the crystals originally formed during crystallization. Therefore, ΔH_f^L usually represented the melting of the crystals formed during crystallization, whereas ΔH_f^H was probably due to the melting of crystals of higher stability formed by the recrystallization of crystals initially obtained. Moreover, the area of ΔH_f^L increased with increasing isothermal temperature because a higher degree of perfection was achieved in the crystals initially obtained, although the area of ΔH_f^H decreased with increasing isothermal temperature. This was due to the melting of crystals formed during recrystallization, and the results obtained were assumed to be because the same degree of per-

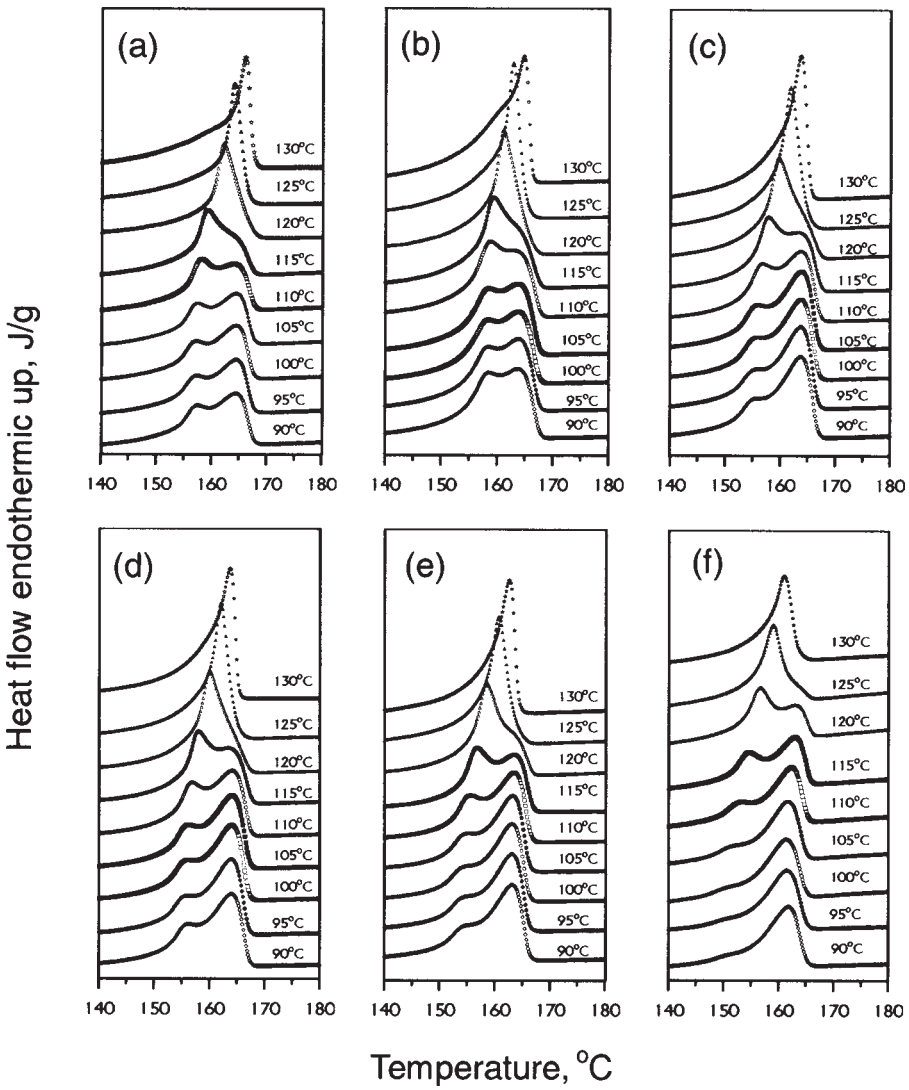

Figure 1 Melting endotherms of iPP/aPP blends after isothermal crystallization for 120 min at different isothermal temperatures: (a) iPP-100, (b) iPP-90, (c) iPP-80, (d) iPP-70, (e) iPP-50, and (f) iPP-30.

fection was achieved in recrystallized crystals. ΔH_f^L and the melting temperature of the lower temperature endotherm (T_m^L) remained almost constant at temperatures below 105°C, and then, ΔH_f^L and T_m^L increased at higher isothermal temperatures. This indicated that a higher degree of perfection was achieved in the crystals due to the higher thermodynamic mobility of iPP molecules necessary for the recrystallization to take place. ΔH_f^L and T_m^L did not changed at temperatures below 105°C, which implied that the previous thermal history or degree of perfection achieved may have been the same. The melting temperature of the higher temperature endotherm remained unchanged, whereas ΔH_f^H decreased with increasing isothermal T_c.

An increasing T_c led to the promotion of a higher degree of perfection of crystals and fewer iPP chains for recrystallization to take place at higher temperatures, so the obtained crystals were more perfect than those formed at lower isothermal temperatures. However, the existence of double melting endotherm peaks in the DSC profiles may have resulted because of the following: first, the presence of two different crystal structures, the presence of two different thicknesses of crystal lamellae with the same type of crystal formed at the isothermal crystallization conditions,[36] and second, the simultaneous melting–reorganization/recrystallization–remelting of the lamellae originally formed during the crystallization process.[37] The WAXD results, shown later in Figure 8, indicated that the γ-form coexisting with the α-form crystal structures for pure iPP and iPP blends with lower amounts of aPP during the crystallization process. However, the results of iPP blends with larger amounts of aPP show that only the α-form crystal structure was observed. Thus, the

occurrence of the double melting peaks may have mainly been caused by coexistence with the different types of crystal structures and different crystal thicknesses with simultaneous melting–reorganization/recrystallization–remelting of the lamellae during the heating trace. The double endotherms were attributed to the recrystallization of less perfected and more perfected α- and/or γ-form crystals and presented a morphology transition temperature at $T_c = 120^\circ$C. However, below this transition temperature, imperfect α- and γ-form crystals were obtained and led to two endotherms. However, above this transition temperature, more perfect α- and γ-form crystals were formed, in which only a single endotherm was observed. The development of X_c of the iPP blend explained that the diluent aPP molecules suppressed the entanglement between iPP molecules and promoted the mobility of iPP molecules during crystallization. However, with larger amounts of aPP, the decreasing X_c of the iPP blends may have been the larger amount of diluent aPP action suppressed the concentration of the nucleus more and inhibited the iPP molecular from molten region diffusing to the surface of nucleus during crystallization.[31]

Isothermal crystallization kinetics

On the basis of the previous results, therefore, this study was conducted to measure the effects of aPP content and isothermal temperature on the crystallization kinetics and morphology development of the iPP blends. Generally, analysis of isothermal crystallization kinetics of polymer and polymer blends is performed with a classical Avrami equation, as given in eq. (1):[34,35]

$$1 - X(t) = \exp(-kt^n) \tag{1}$$

where $X(t)$ is the development of crystallinity at time t and k and n are the crystallization rate constant and the Avrami exponent, respectively. Both k and n depend on the nucleation and growth mechanisms of the spherulites. The fraction of $X(t)$ was obtained from the area of the exothermic peak in the DSC scans; the isothermal crystallization analysis at a crystallization time t was divided by the total area under the exothermic peak, as shown in eq. (2):

$$X(t) = \frac{X_c(t)}{X_c(t=\infty)} = \frac{\int_0^t (dH/dt)dt}{\int_0^\infty (dH/dt)dt} = 1 - \exp(-kt^n) \tag{2}$$

where the numerator is the heat generated at time t and the denominator is the total heat generated until crystallization was complete. t is the time spent during the course of crystallization as measured from the onset of crystallization. To deal conveniently with the operation, eq. (1) is usually rewritten in a double logarithmic form as follows:

$$\log\{-\ln[1 - X(t)]\} = \log k + n \log t \tag{3}$$

According to eq. (3), when $\log\{-\ln[1 - X(t)]\}$ is plotted against $\log t$, the n and k values can be directly obtained as the slope and the intercept, respectively, of the linear plots of $\log\{-\ln[1 - X(t)]\}$ against $\log t$. On the basis of eq. (1), if the time the polymer spends from the beginning of the crystallization process to the time at which a certain amount of relative X_c has developed is known, k can also be directly calculated if eq. (1) is rearranged as follows:

$$k = \frac{-\ln[1 - X(t)]}{t^n} \tag{4}$$

If $X(t) = 0.5$, eq. (4) converts in to a more familiar equation, which is rewritten as follows:

$$k = \frac{\ln 2}{t_{1/2}^n} \tag{5}$$

To analyze the effects of the aPP content and isothermal temperature on the crystallization kinetics for the iPP blends, the exothermic profiles of iPP-100, iPP-80, and iPP-30 at various T_c's are shown in Figure 2. As the results indicate, the time to reach the maximum degree of crystalline order in the iPP blends increased with increasing T_c. Generally, the time needed to reach the maximum degree of crystalline order of iPP blends was slower than that of iPP-100. However, interestingly, if the temperature was lower than 120°C, the time needed to reach the maximum degree of crystalline order of the iPP-80 was shorter than that of pure iPP and iPP-30; however, the amount of nuclei per unit area in iPP-80 was higher than that in pure iPP under the same conditions (as shown later in Fig. 6). These results indicate that the crystallization mechanism of iPP-80 must have been different that of iPP-100 and iPP-30. Interestingly, at lower T_c's, the viscosity of iPP molecules was high due to more entanglements between iPP chains; therefore, the small amount of molten aPP molecules acting as the diluent role for iPP molecules promoted the chain mobility of iPP and increased the free volume between iPP chains, and so this led to an increase as the growth rate of iPP during crystallization.[31] The effect of aPP content and isothermal temperature on the relative X_c for the iPP blends with crystallization time is plotted in Figure 3. The results indicate that the overall crystallization mechanism of the iPP blends showed a sigmoidal curve characterized by a primary crystallization process during the initial stage and by a secondary

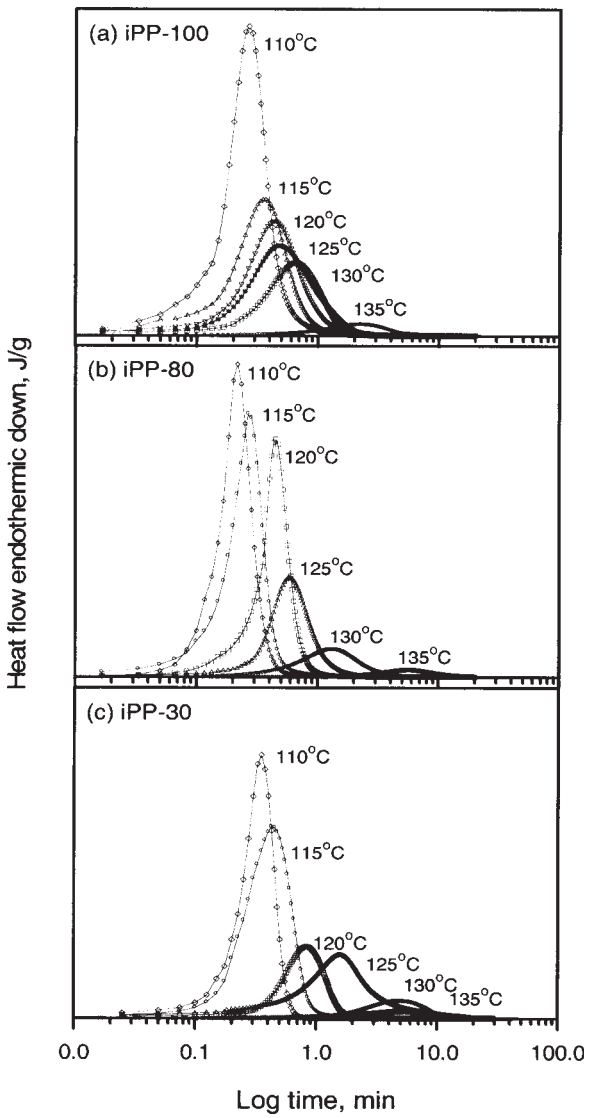

Figure 2 Effect of aPP content and isothermal T_c on the exothermic profiles for the iPP blends, from left to right: 110, 115, 120, 125, 130, and 135°C.

crystallization process during the later stage. They also show that the crystallization rate of iPP-80 was faster than that of pure iPP at lower T_c values, as shown by the half-time of crystallization ($t_{1/2}$), listed in Table II. As shown in Table II, $t_{1/2}$ of the iPP blends decreased and then increased with increasing aPP content with small and large amounts of aPP; particularly, iPP-80 showed the shortest $t_{1/2}$ for all of the samples at lower T_c values. $t_{1/2}$ is the time to reach the maximum rate of heat flow and corresponds to the change to a slower kinetic process due to the impingement of adjacent spherulites.[38] These results indicate that the nucleation and growth rates of iPP in the iPP blends depended strongly on the aPP content. Therefore, these facts imply that the dispersed aPP molecular played a diluent role in the iPP blends. Further addition of aPP in the iPP led to a drastic increase in $t_{1/2}$ of the iPP blends. However, in higher temperature regions, the thermodynamic or diffuse motion of the iPP chains dominated the crystallization mechanism; therefore, the nucleation and growth rates of the iPP blends decreased with increasing aPP content at higher T_c values.

The effect of aPP content and isothermal temperature on $\log\{-\ln[1 - X(t)]\}$ versus $\log t$ is shown in Figure 4. The overall crystallization rate of polymers was a combination of the growth rate and nucleation rate during crystallization. However, the growth rate was controlled by the diffusion of polymer chains to the nuclear surface, and the nucleation rate was controlled by the specific interfacial energy difference of heterogeneous nuclei and by the concentration of nuclei. The results in Figure 4 show that the overall

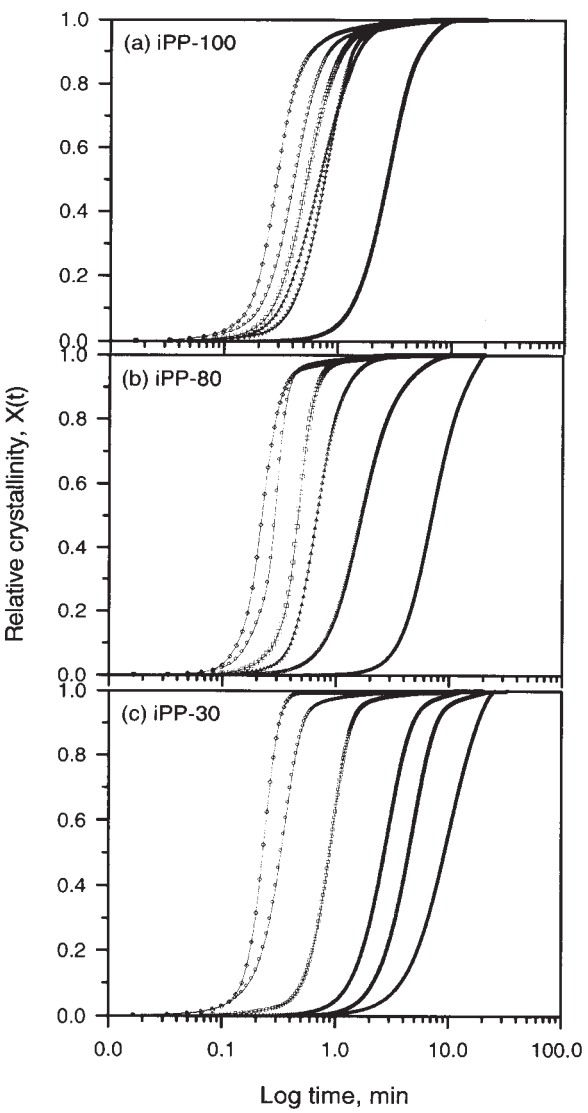

Figure 3 Effect of aPP content and isothermal T_c on relative X_c for the iPP blends, from left to right: 110, 115, 120, 125, 130, and 135°C.

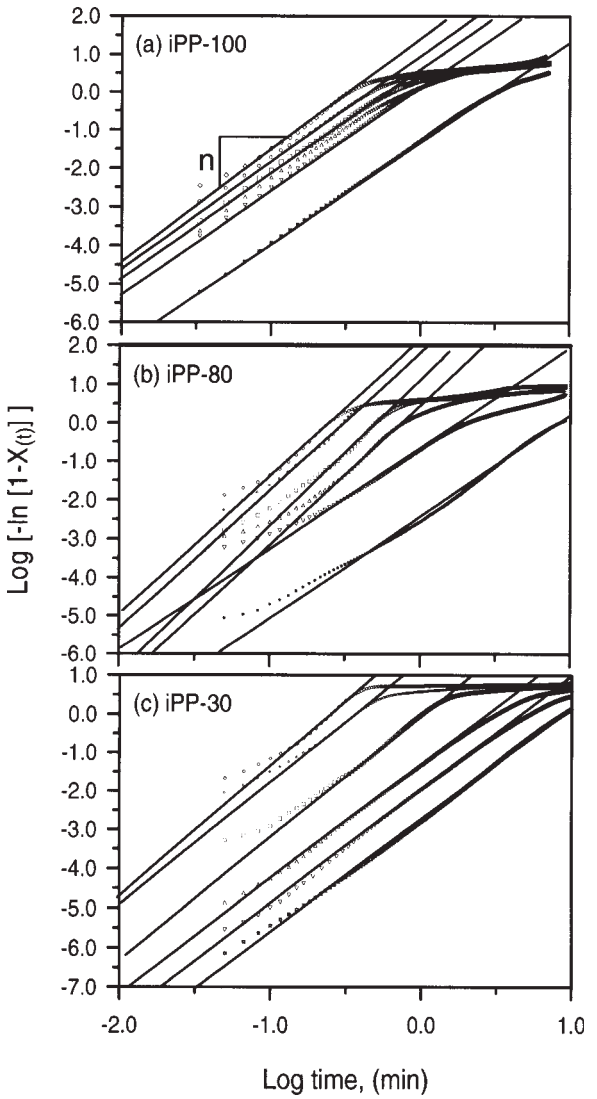

Figure 4 Effect of aPP content and isothermal T_c on the Avrami plots for the iPP blends, from left to right: 110, 115, 120, 125, 130, and 135°C.

crystallization mechanism of the iPP blends gave a nonlinear curve characterized by a primary crystallization process during the initial stage and by a secondary crystallization process during the later stage. The kinetic parameters of the Avrami equation, including n and k, could be determined and fit the initial-stage data.[39] Therefore, the overall crystallization kinetics of the polymer and polymer blend could be analyzed by the observation of rates of the nuclei and growth of crystalline polymers or the rate of formation and growth of a stable nucleus and the rate at which the polymer chains were incorporated into the growing crystalline faces.

In this study, the n values of isothermal crystallization were nonintegral in the range 2–4.[40] Generally, the n value of iPP is about 3–4,[40,41] although some authors have reported the n values in the range of 2[40] to 4[42] for iPP blends. An increase in n is usually attributed in the literature to a change from instantaneous to sporadic nucleation and to an increase in the crystal dimentions.[39] As shown in Table II, the n values were about 2.8 ± 0.2 for iPP-100 and about 3.6 ± 0.5 and 2.5 ± 0.3 for iPP mixtures with smaller and larger aPP contents, respectively. Normally, n values close to 3 of pure iPP indicate an athermal and sporadic nucleation process followed by three-dimensional crystal growth. On the other hand, n values close to 4 indicate a thermal nucleation process followed by three-dimensional crystal growth.[40] The nonintegral of the n value may be considered to be due to the crystal branching, two-stage crystal growth, or mixed growth and nucleation mechanisms.[40,43] Moreover, it was clear that the slope of the plots of $\log\{-\ln[1 - X(t)]\}$ versus $\log t$ for iPP blends remained unchanged until a high degree of conversion was reached at higher T_c values, which implied that secondary crystallization did not play an important role for iPP and iPP blends at higher T_c values. The intercept value of the plots of $\log\{-\ln[1 - X(t)]\}$ versus $\log t$ for iPP blends (k) decreased with increasing T_c. This indicated a decrease in the nucleation and the growth rate constants with increasing T_c; however, k increased with small amounts of aPP and decreased with increasing aPP contents in the iPP blends. These results imply that the overall isothermal crystallization rate of iPP were markedly affected as aPP was added. The isothermal crystallization kinetic parameters are all collected in Table II.

The reciprocal of the half-time ($\tau_{1/2}$) for the iPP blends versus T_c are shown in Figure 5. $\tau_{1/2}$ is the time to reach the maximum rate of heat flow and

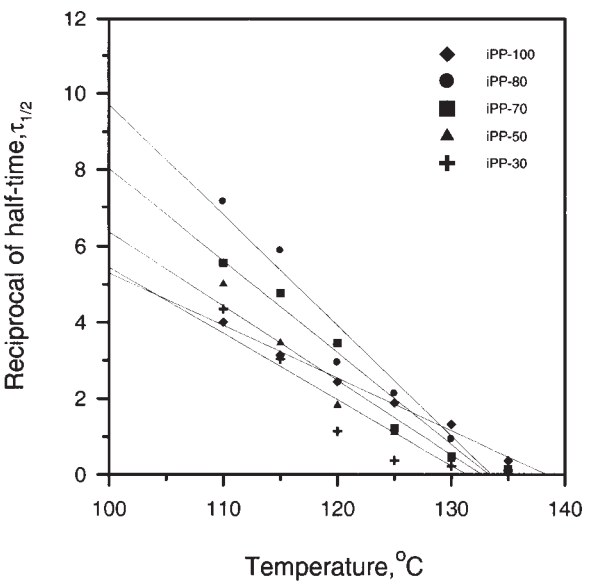

Figure 5 Effect of aPP content and isothermal T_c on $\tau_{1/2}$ for the iPP blends.

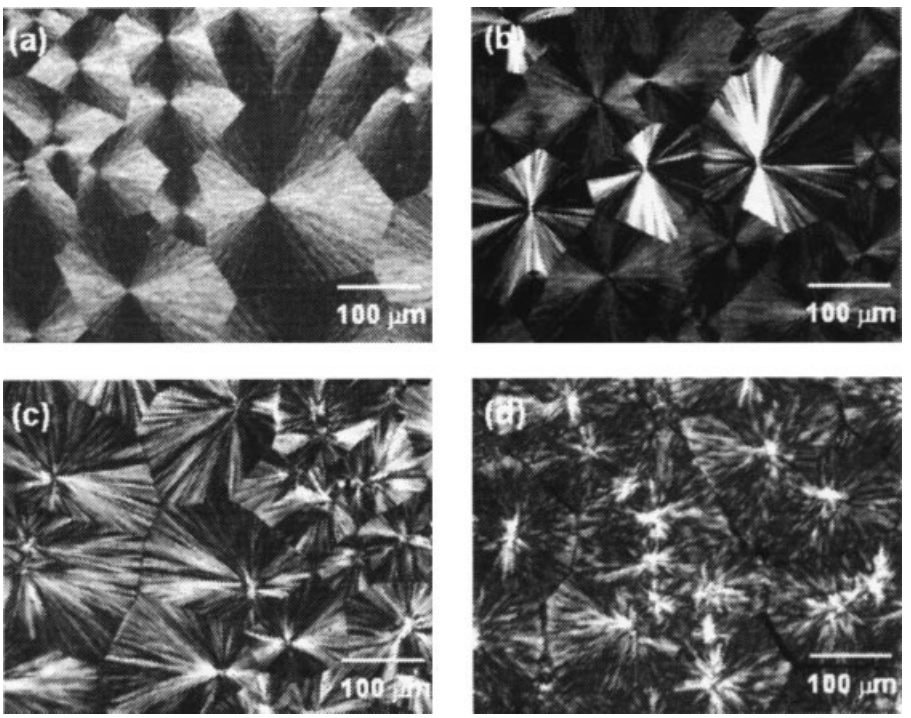

Figure 6 Effect of aPP content on spherulite morphology for the iPP blends at 130°C (magnification = 400×): (a) iPP-100, (b) iPP-80, (c) iPP-50, and (d) iPP-30.

corresponds to the impingement of adjacent spherulites during crystallization. As shown in Table II, $\tau_{1/2}$ of the iPP blends increased and then decreased with increasing aPP at the same T_c. However, $\tau_{1/2}$ of the iPP blends decreased as T_c increased, which implied that the crystallization for the iPP blends was dominated by the nucleation-controlled mechanism.[39] Therefore, these results indicate that the smaller amount of dispersed aPP molecules in the iPP blends acted as the diluent role for iPP molecules and promoted the crystallization rate of iPP. However, with larger amounts of dispersed aPP, $\tau_{1/2}$ of the iPP blends decreased drastically as the larger loading of diluent aPP action suppressed the concentration of the nucleus more and inhibited iPP molecular diffusion to the surface of the nucleus during crystallization.

Morphology development

Figures 6 and 7 show the pictures of the spherulite morphologies of the iPP blends under the polarized optical microscope with a quarter-wave plate (1/4 λ plate) at different aPP contents and isothermal T_c's, respectively. The sign of birefringence of the spherulites was determined by means of a quarter-wave plate located diagonally between crossed polars. Depending on the birefringence, the spherulites could be optically positive or negative. As shown in Figures 6 and 7, the morphologies of the iPP blends depend on both the aPP content and T_c. As shown by POM analyzed for the iPP blends, there was no phase separation in the melt state. This result proved that the aPP molecules were miscible with the iPP chains in the melted state, as reported recently.[31] When the iPP blends were crystallized from the melt, the size and number of spherulites also depended on both the aPP content and T_c. It is interesting that with smaller amounts of aPP, the density of the spherulites in the iPP blends increased with increasing aPP, whereas with larger amounts of aPP, the density of the spherulites in the iPP blends decreased with increasing aPP content, as shown in Figure 6. The effect of aPP on the spherulite morphology of iPP was reported by Keith et al.[32,33] They concluded that with increasing aPP content in iPP/aPP blends, a more open spherulitic texture due to the incorporation of aPP diluent in the interfibrillar regions was observed. However, this study showed increases in the spherulite density or a more dense spherulitic texture with increasing aPP with lower aPP contents, whereas with larger amounts of aPP, there was a decrease in the spherulite density or a more open spherulitic texture with increasing aPP was observed. This fact demonstrates that the diluent aPP molecules promoted the growth rate of iPP because the diluent aPP molecules reduced the entanglement between iPP molecules and increased the mobility of iPP with smaller amounts of aPP and induced a more dense spherulite texture. However,

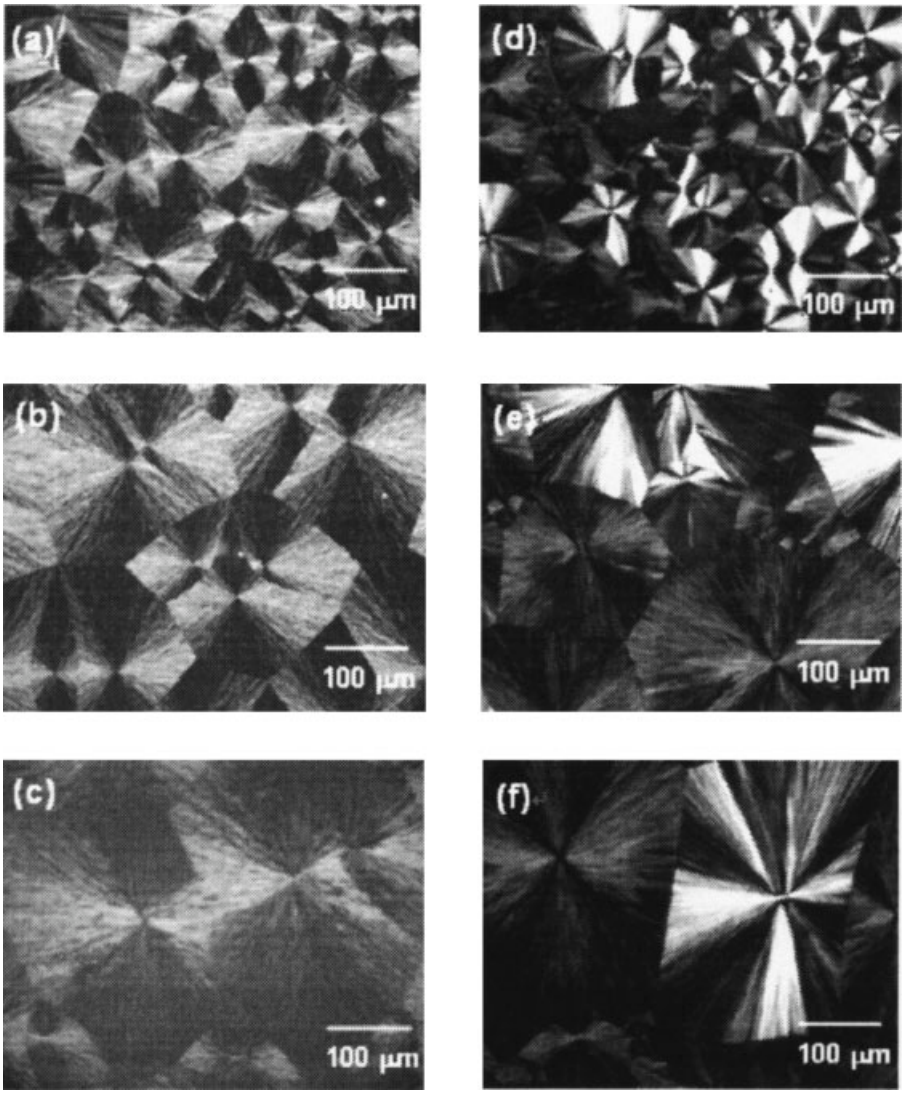

Figure 7 Effect of isothermal T_c on spherulite morphology for the iPP blends (magnification = 400×): (a) 110, (b) 120, and (c) 130°C for iPP-100 and (d) 110, (e) 120, and (f) 130°C for iPP-80.

with larger amounts of aPP, the decreasing X_c of the iPP blends may have been due to the larger amount of diluent aPP action, which suppressed the concentration of the nucleus more and inhibited iPP molecular diffusion to the surface of nucleus during crystallization; therefore, the spherulite morphologies of iPP-50 and iPP-30 showed a more open spherulitic texture, which agreed with the results of Keith and Padden.[32,33]

On the other hand, the signs of birefringence of the spherulites for iPP-100, iPP-50, and iPP-30 presented a negative birefringence, whereas that of the spherulites for iPP-80 presented a mix of positive and negative birefringences (with similar results in iPP-90 and iPP-70), as shown in Figure 6. From several studies reported on the morphologies of melt-crystallized iPP, it is clear that the crystalline morphology of iPP is dominated by a highly characteristic lamellar branching (crosshatching), with radial and tangential lamellae (chains perpendicular and parallel to spherulitic radius, respectively).[7,14–15,44] According to Norton and Keller,[7] the spherulites of iPP-100, iPP-50, and iPP-30 may be dominated by radial lamellae (chains parallel to spherulitic radius), whereas the spherulites of the iPP-80 may be dominated by both crosshatched and radial lamellae (chains perpendicular to spherulitic radius). The different birefringences of spherulites have been linked to lamellae morphology through the balance of crosshatched radial and tangential lamellae or the various feather contents in spherulites.

Figure 7 shows the effect of isothermal T_c on the spherulite morphologies for iPP-100 and iPP-80, respectively. The results indicate that the size of the spherulite increased and the amount of the spherulites decreased as T_c increased. This implies that the

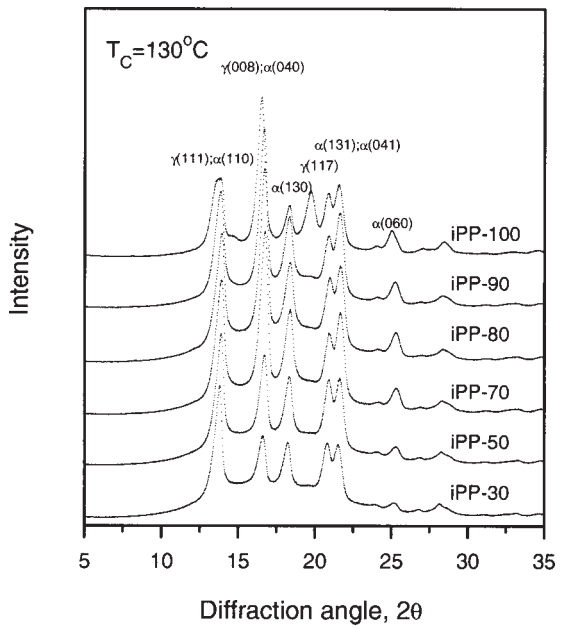

Figure 8 Effect of aPP content on the WAXD intensity patterns for the iPP blends after isothermal crystallization at 130°C.

iPP-100 and iPP blends suppressed the concentration of the nucleus and inhibited iPP molecule diffusion to the surface of the nucleus with increasing T_c because crystallization proceeded for iPP blends dominated by the nucleation-controlled mechanism during crystallization, as discussed previously.

Microstructure

WAXD studies were carried out to obtain information about the crystal microstructure for the iPP and iPP blends. WAXD intensity curves of the iPP blends after isothermal crystallization at 130°C for 120 min are shown in Figure 8. The X-ray diffractograms of samples of the iPP blends showed nearly the α-form diffractograms after they were isothermally crystallized at 130°C. For iPP isothermally crystallized at 130°C, the characteristic peaks of the α form were found at 2θ angles of 14.08° (110), 16.95° (040), 18.5° (130), 21.2° (111), and 21.85° (−131 and 041), as shown in Figure 8.[27,45] Generally, in the typical WAXD intensity pattern of the α form, the intensity of second peak (040) must be smaller than that of first peak (110). In this study, the intensity of the second peak was stronger than the first peak. This fact indicates that other crystal forms have coexisted with the α form of iPP in the iPP blends. The characteristic peaks of the γ form of iPP were also found at 2θ angles of 13.84° (111), 15.05° (113), 16.72° (008), 20.07° (117), 21.2° (202), and 21.88° (026).[27,45] Therefore, these results indicate that the location of the stronger second peak may have been due to the (008) of the γ form coexisting with the (040) of α form of iPP, which implies a lower degree of perfection of the γ-form crystals/triclinic structure coexisting with the α form of iPP at smaller amounts of aPP in the iPP blends during crystallization. However, aPP content in even larger amounts led to a decrease in the γ-form crystallization, which implied that the intensity of second peak was lower than that of the first one for iPP-50 and iPP-30. The developing intensity of the second peak indicated that the aPP molecules acted a diluent on the growth rate of the γ-form crystal because the diluent aPP molecules promoted X_c and/or the crystallization rate of the γ-form crystal of iPP in the iPP blends. This indicated that these diluent aPP molecules were incorporated in the interfibrillar and interlamellar regions to form an unstable γ-form crystal. However, when aPP content was above 50 wt %, the diffraction pattern showed only the α-form diffractogram.

From these results, we determined that the transition from positive to negative spherulites occurred at smaller aPP contents and may have been due to the appearance of coexisting α- and γ-form crystals. Moreover, the highest intensity of the second peak and X_c were obtained for iPP-80; however, the γ-form content almost disappeared for iPP-50. Therefore, the morphology of the spherulites of iPP-50 only showed negative spherulites, whereas that for iPP-80 combined positive with negative spherulites. These result indicated that aPP molecules altered the crystal structures of iPP, favoring the tangential lamellae and, hence, changed the ratio between tangential and radial lamellae or the ratio of featherlike lamellar structures radiating approximately from the centers of the spherulites during crystallization. The morphology transition from a negative to combination of positive and negative spherulites may have been due to appearance of coexisting α- and γ-form crystals of iPP in the iPP blends during crystallization.

In comparison, Figure 9 shows the effect of the isothermal temperature on the WAXD intensity patterns for iPP-100. The results indicate that at higher isothermal temperatures, lower supercooling was more favorable for the γ-form crystal of iPP. The fraction content of the γ-form increased remarkably, whereas that of α-form decreased as the isothermal temperature was increased. This fact indicates that increasing T_c promoted an α- to γ-form transition and induced a higher degree of perfection of the γ-form crystals.[31]

Figure 10(a,b) shows the effect of aPP content on X_c of the iPP blends and normalized X_c of iPP within the iPP blends. Figure 10(a) shows that with increasing aPP content, X_c of the iPP blend increased and then decreased, as shown in Table1. This result indicates that the crystallization ability of iPP was

strongly dependent on the aPP content. At small amounts of aPP, X_c of the iPP blends were higher than that of pure iPP. The developing X_c of the iPP blend showed that the diluent aPP molecules suppressed the entanglement between iPP molecules and promoted the mobility of iPP molecules during crystallization. However, with larger amounts of aPP, the decreasing X_c of the iPP blends may have been due to the larger amount of diluent aPP action that suppressed the concentration of the nucleus more and inhibited the iPP molecules from molten region diffusing to the surface of nucleus during crystallization. In this study, however, aPP was a noncrystalline polymer, and it could not exist in the crystalline structure of iPP. Therefore, aPP must have resided in the noncrystalline regions, that is, the interlamellar and interfibrillar or interspherulitic regions.

Interestingly, the effect of aPP content on the total X_c and the spherulitic density of iPP blends acted as a diluent or plasticizer agent. Therefore, normalized X_c or the crystallizability of the iPP chain within the iPP blends are shown in Figure 10(b). Normalized X_c was calculated with the result of the X_c of iPP blends divided by iPP content within iPP blends, as discussed recently.[31] This result showed that normalized X_c of the iPP molecules within the iPP blends increased with increasing aPP content. This result shows that the aPP molecules promoted the growth rate of iPP because the diluent aPP molecules increased the mobility of iPP and reduced the entanglement between iPP molecules and led to an increase in normalized X_c of iPP during crystallization.

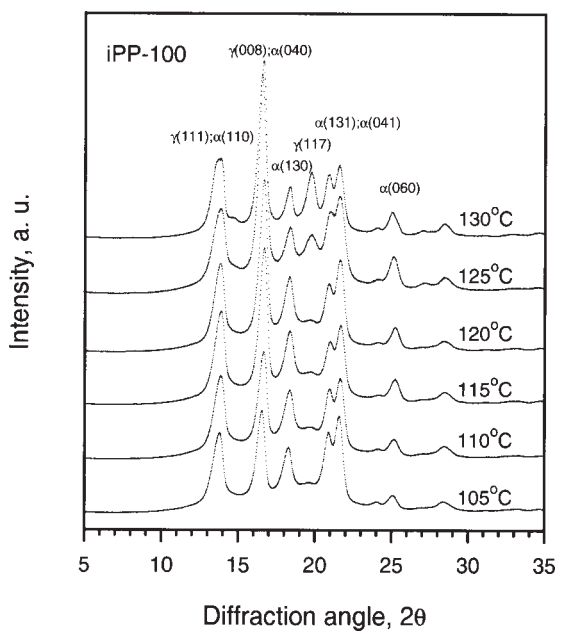

Figure 9 Effect of isothermal T_c on the WAXD intensity patterns for iPP-100.

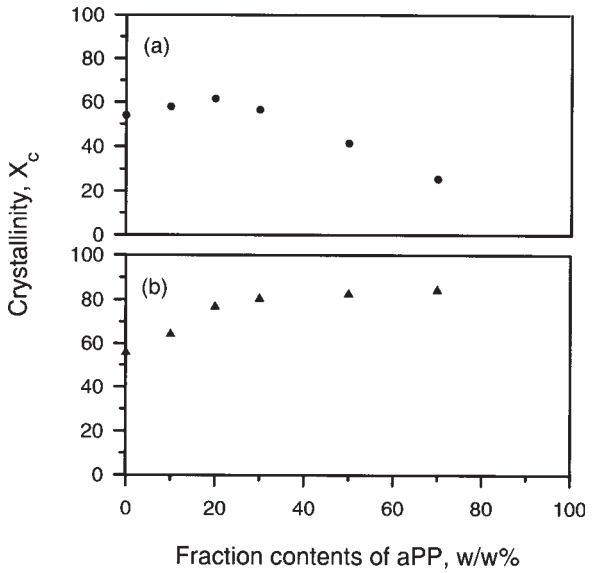

Figure 10 Effect of aPP content on (a) X_c of the iPP blends and (b) normalized X_c of iPP for the iPP blends.

CONCLUSIONS

The crystallization kinetics and morphology development for iPP and iPP blends with aPP were investigated with different aPP contents and isothermal conditions. The crystallization kinetics of iPP blends followed Avrami behavior at early stages of primary crystallization with exponents of 2.75 ± 0.17 for pure iPP and 3.55 ± 0.5 or 2.62 ± 0.3 for iPP blended with smaller or larger amounts of aPP, respectively, over the T_c range studied. The differences in n values were ascribed to different nucleation and crystal growth mechanisms. From these values of n, we established that spherulitic development arose from an athermal and instantaneous nucleation process followed by three-dimensional crystal growth for pure iPP. However, spherulitic development of the iPP blend crystalline phase arose from a thermal and random nucleation process followed by three-dimensional crystal growth with increasing aPP content. From these facts, we concluded that with small amounts of aPP, the aPP molecules promoted the mobility of iPP molecules and reduced the entanglement between iPP molecules and led to an increasing crystallization ability of iPP, whereas with larger amounts of aPP, the decrease in X_c of the iPP blends may have been due to the larger amount of diluent aPP action that suppress the amount of nucleus more and inhibited the iPP molecules from molten region diffusing to the surface of the nucleus during crystallization. This means that the aPP molecules acted as a diluent agent in the iPP phase and had a drastic affect on X_c and structure morphology of the isothermal crystallized iPP.

Because aPP is a noncrystallizable component, it cannot exist in the crystalline structure of iPP; therefore, aPP must reside in the noncrystalline regions of iPP blends. However, with small amounts of aPP, X_c and spherulitic density of the iPP blends were higher than that of pure iPP and presented a lower degree of perfection of the γ-form crystals/triclinic structure coexisting with the α-form of iPP during crystallization. The developing X_c and morphology of the iPP blends showed that the diluent aPP molecular suppressed the amount of entanglement between iPP chains and promoted the mobility of the iPP chain in the amorphous phase during crystallization. However, with larger amounts of aPP, X_c and spherulitic density of the iPP blends decreased, and the reduction in the γ-form crystallization may have been due to the larger amounts diluent aPP molecular action that suppressed the concentration of nucleus more and inhibited the iPP chain from diffusing to the surface of the nucleus during crystallization.

Interestingly, the birefringences of spherulites for iPP-100 and iPP-50 presented a negative profile, whereas that of iPP-80 showed a combination of the positive with negative birefringences, which indicated that aPP molecules altered the spherulite structure of iPP during crystallization and favored the formation of radial lamellae and hence modified the ratio between tangential and radial lamellae. The transition of birefringence of the spherulites from negative to mixed negative and positive spherulites may have been due to the appearance of α- and γ-form crystals coexisting within the iPP blend during crystallization. However, the total X_c of the iPP blends increased and then decreased, whereas the normalized X_c of the iPP molecules within the iPP blends increased with increasing aPP content.[31] Therefore, the aPP content affected the crystallization process of iPP in two opposite directions; that is, it hindered the nucleation rate and promoted the chain motion/growth rate with smaller aPP contents and hindered both the nucleation rate and growth rate at larger aPP contents. The action of these two effects changed the crystal forms from coexisting α and γ forms to the pure α form with increasing aPP content as discussed.

References

1. Natta, G.; Corradini, P. Nuovo Cimento Suppl 1960, 15, 40.
2. Padden, F. J.; Keith, H. D. J Appl Phys 1959, 30, 1479.
3. Keith, H. D.; Padden, F. J.; Walter, N. M.; Wycoff, M. W. J Appl Phys 1959, 30, 1479.
4. Turner-Jones, A.; Aizlewood, J. M.; Beckett, D. R. Makromol Chem 1964, 75, 134.
5. Turner-Jones, A.; Cobbold, A. J. J. Polym Sci 1968, 6, 539.
6. Stocker, W.; Schumacher, M.; Graff, S.; Thierry, A.; Wittmann, J. C.; Lotz, B. Macromolecules 1998, 31, 807.
7. Norton, D. R.; Keller, A. Polymer 1985, 26, 704.
8. Jacoby, P.; Bersted, B. H.; Kissel, W. J.; Smith, C. E. J Polym Sci Part B: Polym Phys 1986, 24, 461.
9. Varga, J.; Karger-Kocsis, J. J Polym Sci Part B: Polym Phys 1996, 34, 657.
10. Samuels, R. J.; Yee, R. Y. J Polym Sci Part A-2: Polym Phys 1972, 10, 385.
11. Morrow, D. R.; Newman, B. A. J Appl Phys 1968, 39, 4944.
12. Kardos, J. L.; Christiansen, A. W.; Bear, E. J Polym Sci Part A-2: Poly Phys 1966, 4, 777.
13. Campbell, R. A.; Phillips, P. J.; Lin, J. S. Polymer 1993, 34, 4809.
14. Mezghani, K.; Phillips, P. J. Polymer 1997, 38, 5725.
15. Mezghani, K.; Phillips, P. J. Polymer 1998, 39, 3735.
16. Addink, E. J.; Beintema, J. Polymer 1961, 2, 185.
17. Binsbergen, F. L.; Lange, B. G. M. Polymer 1968, 9, 23.
18. Brückner, S.; Meille, S. V.; Petraccone, V.; Pirozzi, B. Prog Polym Sci 1991, 16, 361.
19. Meille, S. V.; Brückner, S.; Porzio, W. Macromolecules 1990, 23, 4114.
20. Brückner, S.; Meille, S. V. Nature 1989, 340, 455.
21. Lotz, B.; Wittmann, J. C.; Stocker, W.; Magonov, S. N.; Cantow, H. J. Polym Bull 1991, 20, 209.
22. Lotz, B.; Wittmann, J. C. J Polym Sci Part B: Polym Phys 1986, 24, 1559.
23. Lotz, B.; Graff, S.; Wittmann, J. C. J Polym Sci Part B: Polym Phys 1986, 24, 2017.
24. Phillips, R. A. J Polym Sci Part B: Polym Phys 2000, 38, 1947.
25. Wang, Z. G.; Phillips, R. A.; Hsiao, B. S. J Polym Sci Part B: Polym Phys 2000, 38, 2580.
26. Wang, Z. G.; Phillips, R. A.; Hsiao, B. S. J Polym Sci Part B: Polym Phys 2001, 39, 1876.
27. Foresta, T.; Piccarolo, S.; Goldbeck-Wood, G. Polymer 2001, 42, 1167.
28. Torre, J.; Cortázar, M.; Gómez, M.; Ellis, G.; Marco, C. J Polym Sci Part B: Polym Phys 2004, 42, 1949.
29. Torra, F. J.; Cortázar, M. M.; Gómez, M. Á.; Ellis, G.; Marco, C. Polymer 2003, 44, 5209.
30. Silvestre, C.; Cimmino, S.; Lin, J. S. J Polym Sci Part B: Polym Phys 2004, 42, 3368.
31. Chen, J. H.; Tsai, F. C.; Nien, Y. H.; Yeh, P. H. Polymer 2005, 46, 5680.
32. Keith, H. D.; Padden, F. J. J Appl Phys 1964, 35, 1270.
33. Keith, H. D.; Padden, F. J. J Appl Phys 1964, 35, 1286.
34. Avrami, M. J Chem Phys 1940, 8, 212.
35. Avrami, M. J Chem Phys 1941, 9, 177.
36. Cebe, P.; Hong, S. D. Polymer 1986, 27, 1183.
37. Holdsworth, P. J.; Turner-Jones, A. Polymer 1971, 12, 195.
38. Bodor, G. Structural Investigation of Polymers; Horwood: Chichester, England, 1991.
39. Wunderlich, B. Macromolecular Physics; Academic: New York, 1976; Vol. 1, p 21.
40. Wunderlich, B. Macromolecular Physics; Academic: New York, 1976; Vol. 2, p 115.
41. Godovskii, Y. K. Polym Sci USSR 1969, 11, 2423.
42. Carfagna, C.; Derosa, C.; Guerra, G.; Petraccone, V. Polymer 1984, 25, 1462.
43. Jonsson, H.; Wallgren, E.; Hult, A.; Gedde, U. W. Macromolecules 1990, 23, 1041.
44. Varga, J. J Mater Sci 1992, 27, 2557.
45. Phillips, R. A.; Wolkowicz, M. D. In Polypropylene Handbook; Moore, E. P., Ed.; Hanser: Munich, 1996; p 113.